Pharm Res (2013) 30:1263–1280
DOI 10.1007/s11095-012-0965-4

RESEARCH PAPER

Effects of Ionic Strength and Sugars on the Aggregation Propensity of Monoclonal Antibodies: Influence of Colloidal and Conformational Stabilities

Shuntaro Saito • Jun Hasegawa • Naoki Kobayashi • Toshiaki Tomitsuka • Susumu Uchiyama • Kiichi Fukui

Received: 31 August 2012 / Accepted: 13 December 2012 / Published online: 15 January 2013

ABSTRACT

Purpose To develop a general strategy for optimizing monoclonal antibody (MAb) formulations.

Methods Colloidal stabilities of four representative MAbs solutions were assessed based on the second virial coefficient (B_2) at 20°C and 40°C, and net charges at different NaCl concentrations, and/or in the presence of sugars. Conformational stabilities were evaluated from the unfolding temperatures. The aggregation propensities were determined at 40°C and after freeze–thawing. The electrostatic potential of antibody surfaces was simulated for the development of rational formulations.

Results Similar B_2 values were obtained at 20°C and 40°C, implying little dependence on temperature. B_2 correlated quantitatively with aggregation propensities at 40°C. The net charge partly correlated with colloidal stability. Salts stabilized or destabilized MAbs, depending on repulsive or attractive interactions. Sugars improved the aggregation propensity under freeze–thaw stress through improved conformational stability. Uneven and even distributions of potential surfaces were attributed to attractive and strong repulsive electrostatic interactions.

Conclusions Assessment of colloidal stability at the lowest ionic strength is particularly effective for the development of formulations. If necessary, salts are added to enhance the colloidal stability. Sugars further improved aggregation propensities by enhancing conformational stability. These behaviors are rationally predictable according to the surface potentials of MAbs.

KEY WORDS aggregation · analytical ultracentrifugation sedimentation equilibrium · colloidal and conformational stabilities · monoclonal antibody · second virial coefficient

ABBREVIATIONS

AUC-SE	analytical ultracentrifugation sedimentation equilibrium
B_2	second virial coefficient
B_{22}	osmotic second virial coefficient
CDR	complementarity determining region
DLS	dynamic light scattering
DSC	differential scanning calorimetry
MAb	monoclonal antibody
PDB	protein databank
T_m (T_{max})	apparent unfolding temperature

INTRODUCTION

Aggregation of therapeutic proteins is a crucial issue because of the potential risk of this inducing adverse immunogenic responses (1). It is therefore necessary to minimize the aggregation of therapeutic proteins such as monoclonal antibodies (MAbs) during their life cycle, including their manufacture, storage, transfer, and administration to

Electronic supplementary material The online version of this article (doi:10.1007/s11095-012-0965-4) contains supplementary material, which is available to authorized users.

S. Saito · N. Kobayashi · T. Tomitsuka
Analytical & Quality Evaluation Research Laboratories
Daiichi Sankyo Co., Ltd., 1-12-1, Shinomiya
Hiratsuka-shi, Kanagawa 254-0014, Japan

J. Hasegawa
Biologics Research Laboratories
Daiichi Sankyo Co., Ltd., 1-2-58, Hiromachi
Shinagawa-ku, Tokyo 140-8710, Japan

S. Saito · S. Uchiyama · K. Fukui (✉)
Department of Biotechnology, Graduate School of Engineering
Osaka University, 2-1 Yamadaoka
Suita, Osaka 565-0871, Japan
e-mail: kfukui@bio.eng.osaka-u.ac.jp

patients. However, appropriate control of aggregation is a considerable challenge because of the contributions of multiple aggregation pathways (2–4). Knowledge of aggregation mechanisms has accumulated, and models of the aggregation pathways have been proposed (3,5–8). Two types of stability, colloidal and conformational, are related to the formation of aggregates in these models. Colloidal stability is a measure of molecular dispersity (9,10), which is determined by the marginal balance of attractive and repulsive intermolecular interactions among protein molecules. The Derjaguin–Landau–Verwey–Overbeek (DLVO) theory states that for a solution with high colloidal stability, the repulsive forces arising from electrostatic interactions among molecules are greater than the attractive forces attributed to van der Waals interactions (11). In contrast, the conformational stability is defined as the free energy difference between the folded and unfolded states (ΔG_{FU}) (3,12,13). A higher ΔG_{FU} indicates greater conformational stability, because the population of unfolded states is smaller. Unfolded states consist of an ensemble of various structures. For example, hydrophobic residues that are buried in the native structure are exposed, making them prone to aggregate. A protein with higher conformational stability is therefore expected to possess a lower propensity to aggregate. The unfolding of the protein in the native state is induced by two major environmental factors as follows: a temperature increase and/or contact with a hydrophobic interface, which triggers aggregation. In practice, multiple pathways independently, additively, or synergistically contribute to the formation of aggregates.

Colloidal and conformational stabilities have been assessed for optimizing formulations, stabilizing proteins, and determining the mechanisms of aggregation (5,7,8,14,15). In these studies, several parameters were used as indicators of colloidal and conformational stabilities. The osmotic second virial coefficient (B_{22}) is one of the parameters that represents the degree of intermolecular interactions in relatively dilute solutions and can be used to assess colloidal stability. The second virial coefficient, B_2 ($B_2 = B_{22}/M_W^2$), can be determined experimentally using static light scattering (SLS), self-interaction chromatography (SIC), or analytical ultracentrifugation sedimentation equilibrium (AUC-SE). SLS is used most frequently for the evaluation of B_2 (16,17). SIC provides values of B_2 comparable to those determined using SLS in a shorter time and with a smaller amount of sample (18–20). AUC-SE is a conventional but powerful method for the determination of B_2 from the concentration dependence of the apparent molecular weight ($M_{W,app}$) of a protein in solution (15,21). Winzor *et al.* reported that B_2 values evaluated from AUC-SE data represent specifically intermolecular interactions (22). Positive and negative B_2 values imply the presence of repulsive and attractive intermolecular interactions, respectively (14,23).

Electrostatic interactions have recently received much attention (24–27), because colloidal stability is largely modulated by ionic strength and the species of ion. Zeta potential and/or net charge have been evaluated to characterize the electrostatic potential of proteins. Zeta potential is estimated from electrophoretic mobility measured under an applied electric field using the Henry equation (28,29), and the zeta potentials of MAbs are known (30,31). The effective net charge of a protein is derived from its electrophoretic mobility and diffusion constant, from which protein net charge is calculated based on Debye-Hückel-Henry model (32). The electrostatic properties of a protein can be accurately determined by its net charge (32,33). Because the net charge of a protein is a global attribute that depends on the properties of protein, the properties of the counter ion and co-ions, and the behavior of ions in the vicinity of proteins, this parameter is highly complex. Therefore, it is necessary to determine the actual charge of the protein (32,34).

The conformational stability of a protein is evaluated using several approaches, including differential scanning calorimetry (DSC), circular dichroism spectroscopy (35,36), and differential scanning fluorimetry. The apparent unfolding temperature (T_m), or the temperature at which unfolding begins (T_{onset}), partly reflects ΔG_{FU} at temperatures not far from the unfolding temperature. DSC, in particular, enables direct thermodynamic assessment of the conformational stability per domain based on the endothermic reaction accompanying unfolding. B_2 and T_m and/or T_{onset} provide good correlations with aggregation propensities, but exceptions have been frequently observed (5,7). Further, it should be noted that the relationship between colloidal and conformational stabilities and long-term storage stability remains uncertain. Nevertheless, in practice, the assessment of long-term storage stability, which is time consuming and requires a large amount of sample, is an essential strategy for evaluating aggregation propensity. In this context, the developments of high-throughput and sensitive techniques are urgently needed for the estimation of aggregation propensity.

In our previous study, we focused on colloidal stability and investigated the correlations between B_2 from AUC-SE measurements of solutions at concentrations less than 10 mg/mL and aggregation propensity or viscosity enhancement in high-concentration formulations (≥100 mg/mL) for three different MAbs (5). The pH dependences of B_2 were qualitatively correlated with the aggregation propensity of the three MAbs, indicating that increases in aggregation can

be attributed to a reduction in colloidal stability. However, the correlation became insignificant when the B_2 values were negative. Thus, different MAbs exhibited different aggregation propensities even if the B_2 values were the same.

In the present study, we aimed to develop a general strategy for the development of MAb formulation through the proper assessment of colloidal and conformational stabilities. To assess these stabilities, we studied four MAbs, namely, MAb-A, MAb-B, MAb-C, and MAb-D, which differ in the amino acid sequences of their variable regions. The colloidal stabilities were assessed in terms of B_2 from AUC-SE, k_D from dynamic light scattering (DLS), and zeta potential and net charge from electrophoretic light scattering.

We focused first on the effect of salts on the intermolecular interaction in terms of the electrostatic interaction. Our findings emphasize the great importance of measuring the type of electrostatic interaction. Furthermore, electrostatic repulsion and attraction were determined from electrostatic potential surfaces simulated according to the Poisson–Boltzmann equation using the structure of IgG1 as a model. Second, we assessed the effect of sugars to represent excipients in protein pharmaceutics. Sugars enhance conformational stability through a preferential solvation mechanism in solution (37,38). However, to our knowledge, the contribution of sugars to colloidal stability is unknown. Finally, we confirmed the contribution of colloidal and conformational stabilities to aggregation propensities in the presence of different stress factors. Based on our findings, we propose an effective strategy for optimizing formulations.

MATERIALS AND METHODS

Materials

Humanized monoclonal antibody A (IgG1 subclass, MAb-A), B (IgG1 subclass, MAb-B), C (IgG1 subclass, MAb-C), and D (IgG1 subclass, MAb-D) were produced and highly purified at Daiichi Sankyo Co., Ltd., Tokyo, Japan. All the MAbs were humanized IgG_1. The theoretical isoelectric points (pI) of MAb-A, MAb-B, MAb-C, and MAb-D were 6.7, 8.9, 8.8, and 9.0 respectively. The molecular weights (M_W) of MAb-A, MAb-B, MAb-C, and MAb-D, calculated from amino acid sequences with two oligosaccharide chains ($M_{W,cal}$), were 150, 147, 148, and 151 kDa, respectively. All the MAbs were dialyzed against appropriate initial buffers (pH 5, 6, 7, and 8) before use, and the concentrations were determined based on the absorbance at 280 nm. The MAbs were diluted to adjust the concentration to 20 mg/mL for storage. Each MAb in the initial buffer was diluted two-fold with the necessary buffer to give a solution concentration of 10 mg/mL prior to each experiment. NaCl was purchased from Wako Pure Chemical Industries, Ltd. (Osaka, Japan), and sodium phosphate and sodium acetate were purchased from Kanto Chemical Co. (Tokyo, Japan). Sucrose, sorbitol, and trehalose were purchased from Merck (Darmstadt, Germany), Roquette Co. (Lestern, France) and Hayashibara Co. (Okayama, Japan), respectively.

Formulations

The initial buffer at pH 5 was 10 mM sodium acetate buffer. The initial buffers at pH 6, pH 7, and pH 8 were 10 mM sodium phosphate buffer. The initial buffers for MAb-A additionally contained 30 mM NaCl because the solution become opaque at an NaCl concentration less than 30 mM. These initial buffers correspond to the lowest ionic strength. Buffers designated as +70, +140, and +300 mM NaCl each contained the indicated concentration of NaCl. The buffers represented as +Sorbitol, +Sucrose, and +Trehalose contained 5% sorbitol, 10% sucrose, and 10% trehalose, respectively under the lowest ionic strengths.

Analytical Ultracentrifugation Sedimentation Equilibrium Studies

AUC-SE was conducted using a Proteome XL-I (Beckman Coulter, Inc., Brea, CA, USA). A volume of 60 μL of each solution at 1, 5, or 10 mg/mL, was placed in sample sectors with six holes, a charcoal-filled epon centerpiece (1.2 cm) with sapphire windows, and 60 μL of reference solutions were added to the reference sectors. The runs were carried out at 11 000 rpm at 20°C using an An-50Ti rotor. The concentration gradient was monitored based on Rayleigh interference (IF) optics. The concentration gradients were acquired at 2-h intervals and were judged to be at equilibrium when three successive gradients were completely superimposed. The $M_{W,app}$ was estimated by nonlinear least-squares fitting, using OriginLab software, ver 6.04 (OriginLab Corporation, Northampton, MA, USA) (5). The partial specific volume and solvent density were calculated using Sednterp software (39) or literature values. The partial specific volumes of MAb-A, MAb-B, MAb-C, and MAb-D, according to their amino acid compositions, were 0.7261, 0.7272, 0.7275, and 0.7287 cm^3/g, respectively.

B_2 was obtained from the slope of the plot of the inverse of $M_{W,app}$ against the concentration, according to Eq. 1:

$$\frac{1}{M_{W,app}} = \frac{1}{M_W} + 2B_2c \tag{1}$$

$$B_{22} = B_2 \times {M_W}^2 \tag{2}$$

where M_W is the weight-average molecular weight at infinite dilution and c is the initial loading concentration. B_{22} was obtained using Eq. 2 (22).

Estimation of Concentration Dependence of Diffusion Coefficient by Dynamic Light Scattering

Samples of volume 15 μL of 2.0, 4.0, 6.0, 8.0, and 10 mg/mL sample solutions (after filtration with a 0.22-μm filter) were applied to 384-well optical clear-bottomed microtiter plates. Following centrifugation at 135*g* for 3 min to remove bubbles, the diffusion coefficient was measured using a DynaPro Plate Reader (Wyatt Technology Corp., Santa Barbara, CA, USA) at 20°C. The interaction parameter (k_D) was calculated using Eq. 3, where D_m is the measured diffusion coefficient, D_S is the diffusion coefficient at infinite dilution, and c is the MAb concentration (mg/mL).

$$D_m = D_S(1 + k_D c) \tag{3}$$

Determination of Zeta Potential and Net Charge

Approximately 600 μL of 2.0 mg/mL sample solution (after filtration through a 0.22-μm filter) was injected using a syringe pump. The zeta potential, ζ, was measured using a Mobius mobility instrument (Wyatt Technology Corp.) at 20°C equipped with an ATRAS N_2 gas pressure device (Wyatt Technology Corp.). The ATRAS device prevents the generation of air bubbles by pressurizing the solution and enables ζ measurements in the presence of high concentrations of salts. The solution state was monitored by DLS during the ζ measurements to confirm that aggregation and precipitation did not occur.

The equations for calculating zeta potential and net charge are detailed in the Supplementary Material (Equation S1). Briefly, ζ was estimated according to the Henry equation (29,40) using DYNAMICS ver 7.2.3.5 software (Wyatt Technology Corp.) and the electrophoretic mobility and solvent viscosity at 20°C. Solvent viscosity was calculated according to the buffer components using Sednterp software. The net charge, z, was estimated according to a published procedure (34). The self-diffusion coefficient (D_S) using DLS was determined from the extrapolation of diffusion coefficients to zero concentration at different concentrations.

Conformational Stability Assessment by Differential Scanning Calorimetry

DSC studies were performed using a VP capillary DSC system (GE Healthcare, Little Chalfont, UK). Samples of volume 400 μL of 1.0 mg/mL solutions were injected. Changes in the heat capacity (C_P) were measured as the samples were heated from 20 to 100°C at a scanning rate of 60°C/h and a filtering period of 10 s. Data analysis was performed using OriginLab software (OriginLab Corporation). For each sample, a relevant buffer blank containing the same buffer and excipient concentration was subtracted as a reference. Normalized C_P data were corrected for the buffer baseline. An apparent transition midpoint (T_{max}) was determined from the exothermic peak providing the highest C_P.

Stability Studies

Antibody solutions (150 μL, 10 mg/mL) were applied in triplicate to a 96-well polypropylene polymerase chain reaction (PCR) plate with a cap. One plate was analyzed immediately after preparation. Other plates were stored at 40°C for 1, 2, and 4 weeks. Another plate was frozen at −40°C and then thawed at 25°C using an aluminum block matching the shape of the storage plate. This freeze–thaw procedure was repeated 10 times. The aggregation profiles before and after stressing (40°C for 1, 2, and 4 weeks or 10-times freeze–thaw) were analyzed using size-exclusion chromatography (SEC), DLS, and turbidity measurements. There was no detectable change in concentration during storage.

Size-Exclusion Chromatography

Samples were filtered without dilution using 96-well filtration plates (0.45 μm). Size-exclusion chromatography (SEC) analysis was conducted using a TSKgel G3000SW_{XL} (TOSOH Co., Tokyo, Japan) column, and 30 mM phosphate buffer, 300 mM NaCl (pH 6.7) as the mobile phase at a flow rate of 1.0 mL/min and a column temperature of 25°C. A 20-μL sample of each solution was injected into the column. The peak area was monitored at 280 nm using a UV detector. The percentage of aggregates, determined from the sum of the peaks eluted in front of the monomer peak, was estimated by dividing the aggregate peak area by the total area of the peak. The rate of increase in the amount of aggregates, the aggregation rate (percentage per month or percentage per 10-times freeze–thaw cycles), was estimated from least-squares fitting of the aggregation percentages to a linear function.

Dynamic Light Scattering

The samples were diluted to 1 mg/mL with the corresponding formulation buffers and filtered using 96-well filtration plates (0.45 μm). Samples of volume 15 μL were applied to 384-well optical clear-bottomed microtiter plates. Following centrifugation at 135*g* for 3 min to remove large particulates and

bubbles, the average hydrodynamic diameter was measured at 20°C using a DynaPro Plate Reader.

Turbidity Measurements

Samples of volume 20 μL were applied to 96-well optical clear-bottomed microtiter plates without dilution. The turbidity was monitored at 350 nm using a SpectraMax M2 plate reader (Molecular Devices, Sunnyvale, CA, USA). The turbidity of the solution was obtained according to the procedure previously reported (5).

Calculation of Electrostatic Potential Surface

Full-length IgG1 model structures of MAb-A and MAb-B were generated using Discovery Studio software (Accelrys Inc., San Diego, CA, USA). The crystal structure of Anti-HIV-1 GP 120 IgG1 was used as a template (PDB id: 1HZH). The electrostatic potential surfaces were determined according to the Poisson–Boltzmann equation at different pHs and ionic strengths, and +1 and -1 k_BT/e isovalue surfaces were mapped on the model structures. Herein, k_B is the Boltzmann constant.

RESULTS

Measurements of B_2 in Different Solutions

The B_2 values of MAb-A and MAb-B were measured using AUC-SE in the formulations containing different concentrations of NaCl or sorbitol, sucrose, or trehalose to investigate their influence on intermolecular interactions. Evaluations of B_2 values were conducted at two different pHs, at pH 5 and pH 7, where both MAbs showed distinct B_2 values at low ionic strength (Fig. 1a, c); MAb-A showed negative at pH 5 and small negative at pH 7 and MAb-B showed large positive at pH 5 and small negative at pH 7, indicating the presence of different type of the intermolecular interactions (5). This enabled the evaluation of the influence of salt and sugars on the different types of intermolecular interactions.

At the lowest NaCl concentration, negative B_2 values of MAb-A at pH 5 and pH 7 showed the presence of attractive intermolecular interactions. The B_2 values increased as the NaCl concentration increased and inverted from negative to positive values at 300 mM (pH 5) and 70 mM (pH 7). Such dependencies of B_2 on NaCl concentration for MAb-A were

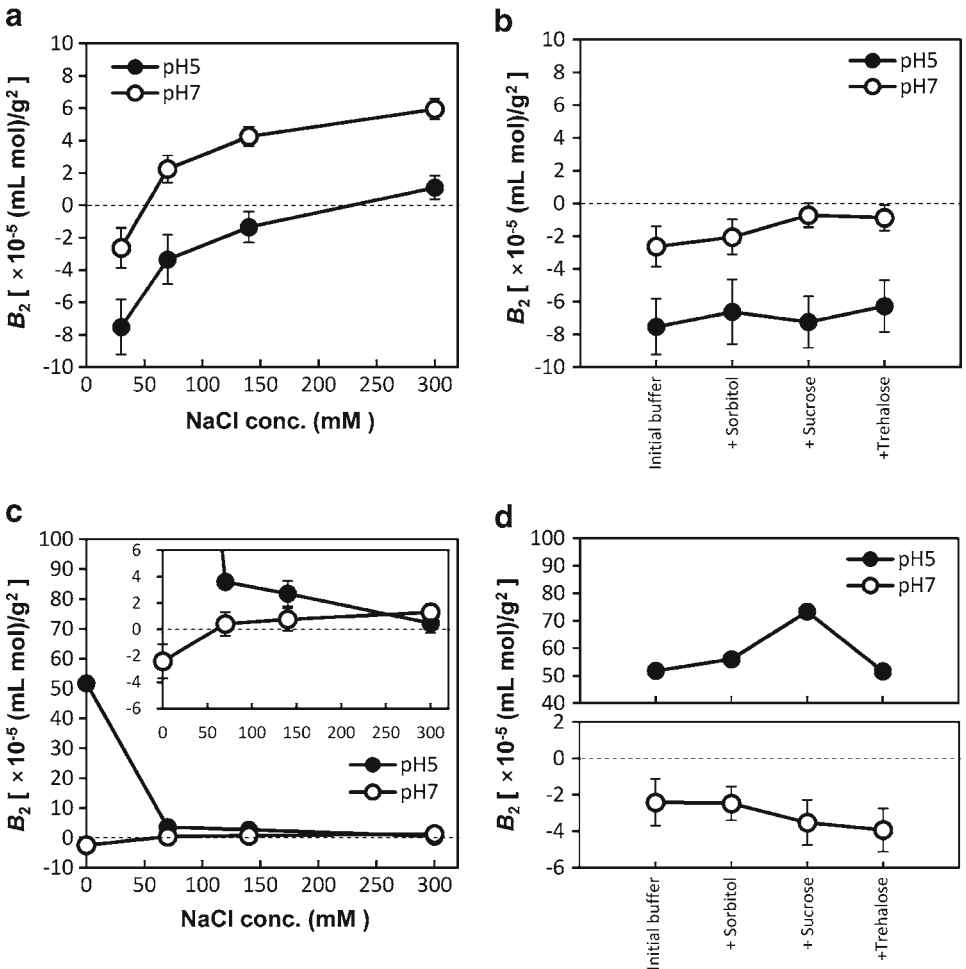

Fig. 1 Second virial coefficient (B_2) for MAb-A (**a**, **b**) and MAb-B (**c**, **d**) in formulations containing different concentrations of NaCl and different sugars were measured by analytical ultracentrifugation sedimentation equilibrium. B_2 was obtained from the concentration dependence of $M_{W,app}$ at three different concentrations, *i.e.*, 1, 5, and 10 mg/mL, in 10 mM AcONa (pH 5) (●) and 10 mM sodium phosphate buffer (pH 7) (○) containing NaCl or sugars as indicated in the figures. The inset in (**c**) is an expanded figure. The lowest ionic strength buffer (initial buffer) contained 30 mM NaCl for MAb-A and no NaCl for MAb-B. The error bar was estimated from three independent experiments under the same conditions.

similarly confirmed at pH 5 and pH 7; however, the B_2 values determined in each salt concentration at pH 7 were higher than those at pH 5, suggesting increased attractive intermolecular interactions at pH 5 than at pH 7. The addition of sugars did not significantly alter the B_2 values, although slight increases in B_2 were observed at pH 7 in the presence of sucrose and trehalose (Fig. 1b).

Figure 1c, d show the B_2 values of MAb-B. The dependence of B_2 on NaCl concentration was similar to that for MAb-A at pH 7, at which the B_2 values were negative in solutions of the lowest ionic strength. The B_2 values increased as the NaCl concentration increased and inverted to positive values in the presence of greater than 70 mM NaCl. In contrast, the B_2 value of MAb-B at pH 5 was high and positive, indicating the presence of strong repulsive intermolecular interactions. The B_2 values of MAb-B decreased strikingly with increasing NaCl concentration, suggesting that NaCl greatly suppressed the repulsive intermolecular interactions. Sucrose enhanced the value of B_2, while sorbitol and trehalose did not.

B_2 Measurements at Low and High Ionic Strengths

The effects on B_2 of changes in the ionic strength were further investigated for four different MAbs (MAb-A, MAb-B, MAb-C, and MAb-D) at pH 5, pH 6, pH 7, and pH 8 at low ionic strength (30 mM NaCl for MAb-A, no NaCl for MAb-B, MAb-C, and MAb-D) or high ionic strength (300 mM NaCl for all MAbs). As shown in Fig. 2a–d, the B_2 values of all the MAbs were affected to some extent as the ionic strength changed, except for MAb-D at pH 7. The negative B_2 values for MAb-A at all pHs, MA-B and MAb-C at pH 7 and pH 8, and MAb-D at pH 8 indicate the presence of weak attractive interactions at low ionic strength. Importantly, negative B_2 values were all inverted to positive values by the addition of 300 mM NaCl. Positive B_2 values were obtained at low ionic strength for MAb-B and MAb-C at pH 5 and pH 6, and MAb-D at pH 5, pH 6, and pH 7. These positive B_2 values were significantly reduced by the addition of 300 mM NaCl, except for MAb-D at pH 7.

Measurement of k_D Using Dynamic Light Scattering

The value of k_D, which is obtained from the concentration dependence of the diffusion constant, D_m, is widely used for estimating the degree of intermolecular interactions (9). The k_D values determined using different formulations were estimated by DLS to compare them with B_2 values obtained using AUC-SE. The k_D values of MAb-A and MAb-B (Table I) showed a linear relationship with those of B_2 obtained by AUC-SE (Supplementary Material Figure S1) in the range $B_2 < 10$ (mLmol)/g^2 with a good correlation

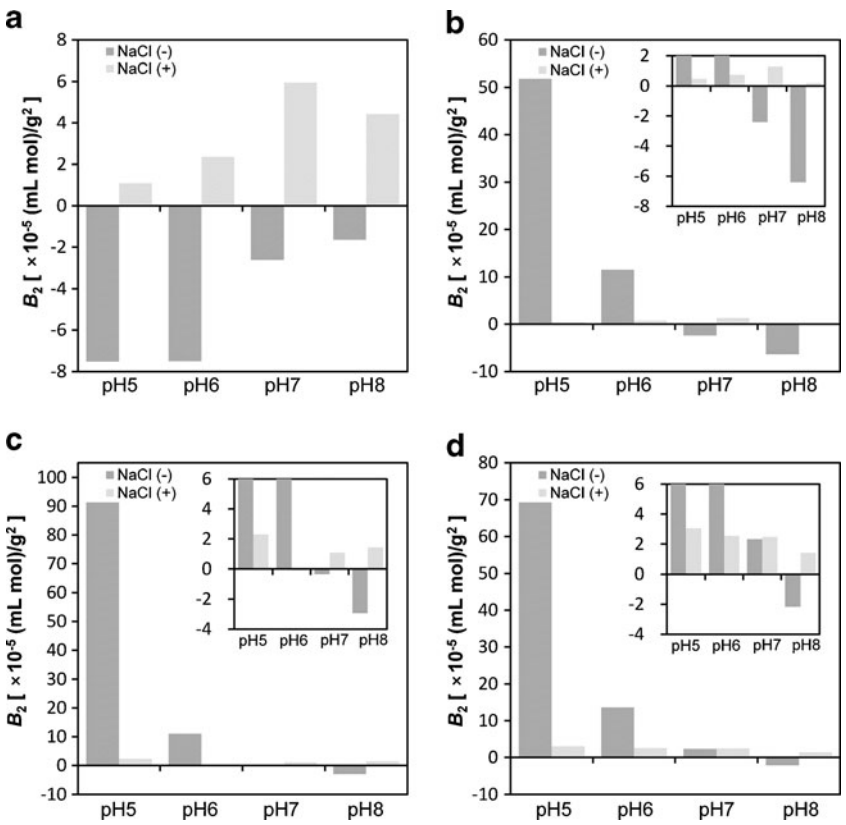

Fig. 2 Second virial coefficient B_2 for MAb-A (**a**), MAb-B (**b**), MAb-C (**c**), and MAb-D (**d**) at four pHs. B_2 was obtained from the concentration dependence of $M_{W,app}$ obtained by analytical ultracentrifugation sedimentation equilibrium at three different concentrations, *i.e.*, 1, 5, and 10 mg/mL, in 10 mM AcONa (pH 5) and 10 mM sodium phosphate buffer (pH 6, pH 7, and pH 8) at the lowest ionic strength (30 mM NaCl for MAb-A and no NaCl for MAb-B, MAb-C, and MAb-D) or at the highest ionic strength (300 mM NaCl).

Table I Influence of Formulations on the Physical Parameters of MAbs

MAb	pH	Formulation	B_2 ($\times 10^{-5}$·(mL·mol)/g^2)	k_D (mL/g)	D_S ($\times 10^{-7}$cm^2/sec)	Zeta potential (mV)	Net charge
MAb-A	5	Initial buffer	-7.53±1.69	-30.5±0.8	4.0±0.0	4.8	4.8
		+70 mM NaCl	-3.35±1.53	-18.7±0.8	3.9±0.0	2.7	2.7
		+140 mM NaCl	-1.36±0.95	-12.8±0.7	4.0±0.0	1.7	1.7
		+300 mM NaCl	1.09±0.73	-7.5±0.9	3.9±0.0	-2.1	-2.1
		Initial buffer	-7.53±1.69	-30.5±0.8	4.0±0.0	4.8	4.8
		+Sorbitol	-6.62±1.97	-26.9±1.5	3.4±0.0	1.2	1.1
		+Sucrose	-7.24±1.57	-30.4±0.6	3.2±0.1	0.0	0.0
		+Trehalose	-6.27±1.58	-29.7±0.1	3.2±0.0	1.3	1.2
	7	Initial buffer	-2.63±1.23	-14.3±0.9	3.9±0.1	-6.8	-7.0
		+70 mM NaCl	2.24±0.84	-7.8±1.0	3.9±0.0	-3.5	-3.7
		+140 mM NaCl	4.26±0.60	-3.7±0.2	3.8±0.0	-2.6	-2.6
		+300 mM NaCl	5.94±0.64	-3.1±0.6	3.7±0.1	1.1	1.0
		Initial buffer	-2.63±1.23	-14.3±0.9	3.9±0.1	-6.8	-7.0
		+Sorbitol	-2.05±1.06	-13.1±1.6	3.3±0.0	-5.9	-6.2
		+Sucrose	-0.73±0.73	-18.3±1.8	2.9±0.1	-2.1	-2.3
		+Trehalose	-0.88±0.78	-17.1±3.5	3.0±0.1	-1.8	-1.7
MAb-B	5	Initial buffer	51.83±2.39	19.6±2.3	4.1±0.0	3.2	3.2
		+70 mM NaCl	3.61±0.47	-6.2±1.2	4.1±0.0	1.5	1.5
		+140 mM NaCl	2.72±0.96	-8.5±0.7	4.1±0.0	1.6	1.5
		+300 mM NaCl	0.47±0.72	-8.8±1.0	4.0±0.0	-1.4	-1.3
		Initial buffer	51.83±2.39	19.6±2.3	4.1±0.0	3.2	3.2
		+Sorbitol	56.02±3.00	18.2±2.2	3.6±0.0	1.5	1.5
		+Sucrose	73.34±3.30	13.3±0.3	3.3±0.0	0.9	0.9
		+Trehalose	51.63±3.72	5.0±1.5	3.4±0.0	1.2	1.1
	7	Initial buffer	-2.41±1.29	-16.0±1.4	4.2±0.0	1.7	1.6
		+70 mM NaCl	0.42±0.89	-8.3±0.7	4.0±0.0	-0.3	-0.2
		+140 mM NaCl	0.76±0.85	-8.6±0.1	4.0±0.0	-0.6	-0.6
		+300 mM NaCl	1.30±0.67	-6.6±1.5	3.9±0.0	-2.3	-2.4
		Initial buffer	-2.41±1.29	-16.0±1.4	4.2±0.0	1.7	1.6
		+Sorbitol	-2.48±0.92	-17.7±1.0	3.6±0.0	1.4	1.7
		+Sucrose	-3.53±1.24	-23.1±0.4	3.3±0.0	0.7	0.7
		+Trehalose	-3.93±1.19	-23.6±1.8	3.3±0.0	1.1	0.9

The lowest ionic strength buffers (initial buffers) contained 30 mM NaCl for MAb-A and no NaCl for MAb-B.
The standard deviation of Z potential and Net charge was approximately less than 2.5 mV and 2.5, respectively

coefficient ($R = 0.95$), providing the following empirical equation:

$$k_D = 1.50B_2M_W - 12.4 \quad (4)$$

The intercept of Eq. 4 has a larger negative value than that calculated from the previously proposed equation, $k_D = 1.06A_2M_W - 8.9$ (28), where A_2 is the secondary virial coefficient estimated from light scattering. Winzor *et al.* reported that A_2 becomes smaller than B_2 because A_2 reflects the combined contributions of protein self-interactions and protein–buffer interactions due to thermodynamic nonideality (22). Theoretically, k_D is composed of a thermodynamic term, B_2, and a hydrodynamic term, $\xi_1 + v$, as shown in the following equation:

$$k_D = 2B_2M_W - (\xi_1 + v) \quad (5)$$

where ξ_1 is the frictional drag of the protein, which increases with increasing protein solvation. The values of ξ_1 and v are positive, making a negative contribution to k_D as evidenced from the larger negative intercept in Eq. 4. In our present study, k_D was negative in several cases, with AUC-SE giving positive values of B_2 (MAb-A at pH 5 with 300 mM NaCl, MAb-B, MAb-C, and MAb-D at pH 5 with NaCl > 70 mM, Table I). Notably, when B_2 exceeded 50×10^{-5} (mLmol)/g^2, the k_D values were smaller than those estimated from Eq. 4. These results suggest that a higher degree of

hydration and/or conformational change increase the frictional drag of the MAb.

Zeta Potential and Net Charge Determination

The values for zeta potential, ζ, and the net charge, z, were determined in the presence of different buffer conditions to assess the relationship of the electric potential surface with B_2. Figure 3a, b and Table I show that MAb-A is positively charged at pH 5 in the presence of the lowest ionic strengths, which is consistent with our previous study (30) and is reasonable when the pI of the MAb-A is considered (pI = 6.7). The charge decreased with increasing NaCl concentration and ultimately changed to a negative value in the presence of high ionic strengths. MAb-A was negatively charged at pH 7 in the presence of the lowest ionic strengths. The negative charge, as was the case at pH 5, decreased as the NaCl concentration increased.

When sugars were added, similar effects on reducing the net charger were observed. Sorbitol, sucrose, and trehalose reduced positive and negative charge at pH 5 and pH 7, respectively. For MAb-B, a positive value was observed in the presence of the lowest ionic strengths at pH 5 and pH 7 (Fig. 3c). The charges decreased as the NaCl concentration increased. The trends in net charge as a function of NaCl concentration were similar at pH 5 and pH 7, but the magnitudes of the positive charges at each NaCl concentration were slightly larger at pH 5 than those at pH 7. The decreases in the net charge of MAb-B observed upon the addition of sugars was not significant (Fig. 3d). The net charge is estimated from the observed electrophoretic mobility of a protein, which is also influenced by the diffusion coefficient, D_s (Supplementary Material Equation S2). In MAb-A at pH 5, D_s decreased while k_D was unchanged in the presence of sucrose and trehalose, implying that protein molecules are more hydrated and become bulky by the addition of these sugars (Table I). The reduction of electrophoretic mobility by sugars, however, cannot be explained only by the reduction of D_s, because D_s was reduced by only four-fifths in the presence of sugars, whereas electrophoretic mobility was reduced to approximately one-fifth, indicating that the addition of sugars reduced the net charge.

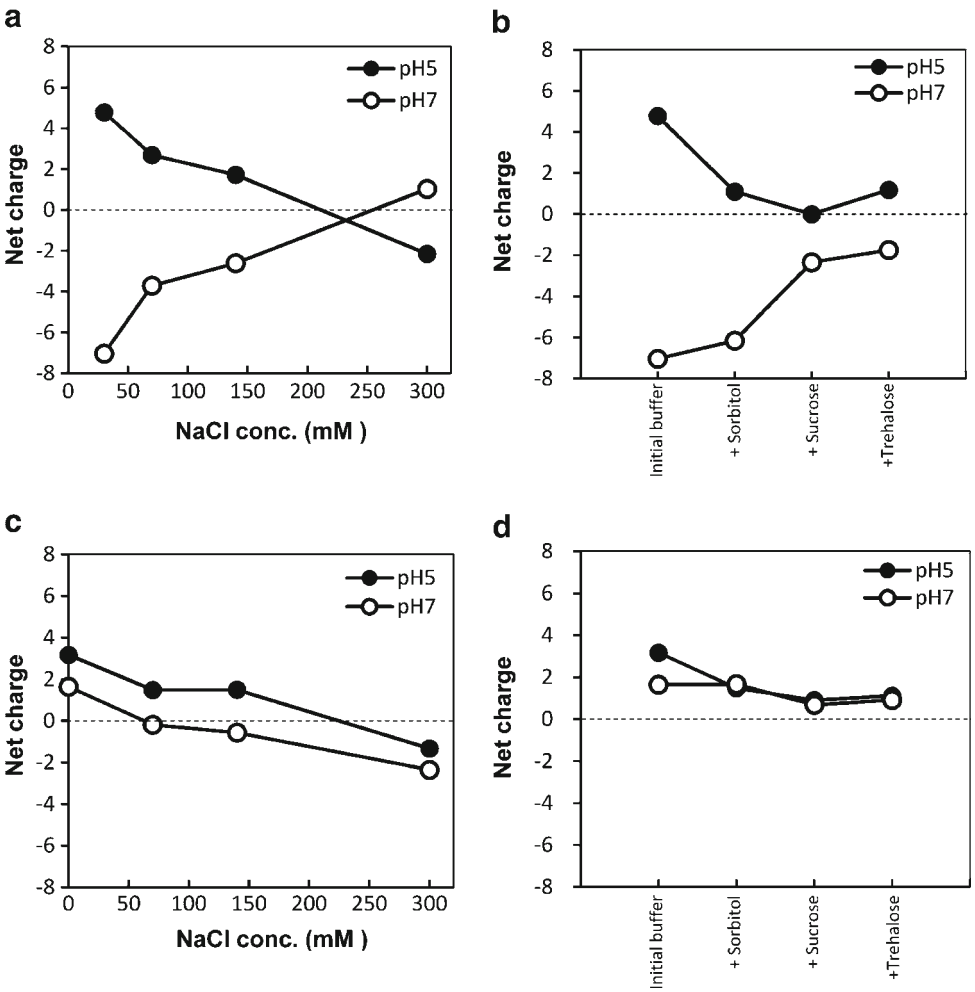

Fig. 3 Net charge for MAb-A (**a**, **b**) and MAb-B (**c**, **d**) in different formulations were calculated from electrophoretic mobility measured at a concentration of 2 mg/mL in 10 mM AcONa (pH 5) (●) and 10 mM sodium phosphate buffer (pH 7) (○) containing NaCl or sugars as indicated in the figures. The lowest ionic strength buffer (initial buffer) contained 30 mM NaCl for MAb-A and no NaCl for MAb-B.

Aggregation Propensities of MAbs during Storage under Accelerated Conditions at 40°C or under Freeze–thaw Stress

Stability assessments under accelerated storage conditions at 40°C or freeze–thaw cycles were conducted for MAb-A and MAb-B at pH 5 and pH 7. In the present study, changes in the aggregate profile were evaluated by SEC, DLS, and turbidity in order to monitor the wide range of aggregates in terms of size (41). SEC is widely used for the evaluation of small soluble aggregates that pass through the SEC column (invisible aggregates of sizes less than 0.1 μm). DLS can detect submicron (subvisible aggregates of size between 0.1 and 1 μm) particles, and turbidity measurements can detect insoluble aggregates (visible aggregates of size greater than 1 μm).

Figure 4 shows the aggregation rates of MAb-A and MAb-B at pH 5 and pH 7. The aggregation rates during storage at 40°C decreased as the NaCl concentration increased for MAb-A at pH 5 (Fig. 4a) and pH 7 (Fig. 4b), and MAb-B at pH 7 (Fig. 4d). These results suggested that NaCl effectively improved the solution stability at 40°C. In contrast, the aggregation rate of MAb-B increased with increasing NaCl concentration at pH 5 (Fig. 4c), indicating a destabilizing effect of NaCl. Under freeze–thaw stress, aggregation was suppressed in MAb-A at pH 7 (Fig. 4b) but accelerated in MAb-B at pH 5 (Fig. 4c) as the NaCl concentration increased. The trends in aggregation rates as a function of NaCl concentration under freeze–thaw stress were in good qualitative agreement with those for storage at 40°C. MAb-A at pH 5 showed the opposite trend in aggregation rates under freeze–thaw stress to those for storage at 40°C. In this case, aggregation was accelerated by freeze–thaw stress but was suppressed for storage at 40°C as the NaCl concentration increased (Fig. 4a). MAb-B at pH 7 showed unique aggregation rate behavior under freeze–thaw stress. The aggregation rates slightly decreased with increasing NaCl concentration from 70 mM to 300 mM, which was the same trend as those for storage at 40°C (Fig. 4d). However, different from the storage at 40°C, the aggregation rate was well suppressed significantly in the absence of NaCl, which was out of line in terms of the relation between aggregation rate and NaCl concentration.

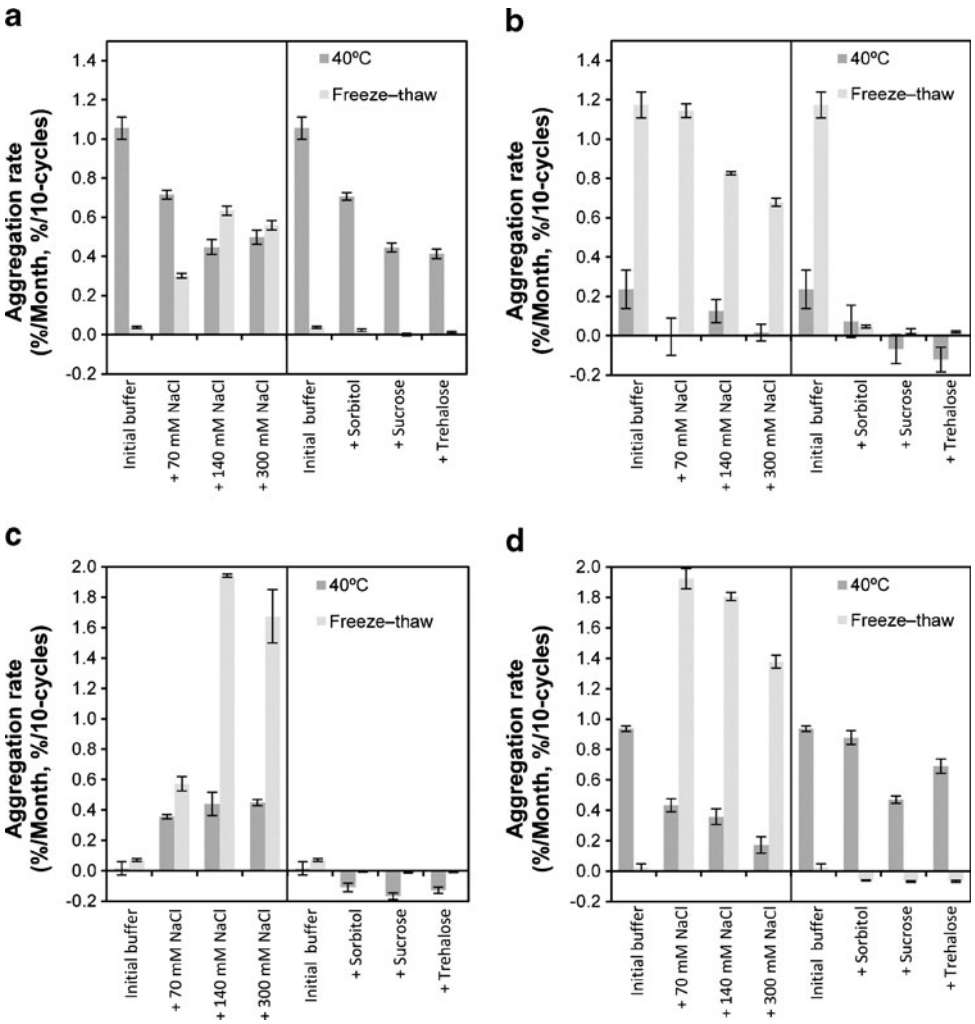

Fig. 4 Quantification of aggregates by size-exclusion chromatography. MAbs were degraded by storing at 40°C for one month and 10 freeze–thaw cycles. The increase in the rate of aggregation was estimated from the increase in the population of aggregates after storage at 40°C (%/month) and freeze–thawing (%/10-cycles) (**a**) MAb-A at pH 5, (**b**) MAb-A at pH 7, (**c**) MAb-B at pH 5, (**d**) MAb-B at pH 7). A negative aggregation ratio indicates a decrease in aggregates compared with the initial measurement. The error bar was estimated from three independent experiments performed under the same conditions.

The addition of sugars slightly improved the aggregation propensities under storage at 40°C for MAb-A at pH 5 and pH 7 (Fig. 4a, b). No significant differences were observed for MAb-B, and the aggregation rates in formulations containing sugars were identical to those under the lowest ionic strength conditions in the absence of sugars (Fig. 4c, d).

In this stability assessment, the initial level of the small soluble aggregates at each pH for MAb-A and MAb-B were almost equivalent regardless of the buffer composition (Supplementary Material Table SI). Both the DLS and turbidity measurements showed that neither submicron particulates nor insoluble aggregates were formed in any of the buffers before and after the acceleration test at 40°C and under freeze–thaw stress.

Conformational Stability Assessment by Differential Scanning Calorimetry

DSC was performed to investigate the contribution of the conformational stability to aggregation propensities in the presence and absence of sugars. T_{max} values, which were defined as the transition temperature of the highest endothermic peak, are summarized in Table II, and their heat capacity curves are shown in Supplementary Material Figure S2. Both MAb-A and MAb-B had higher T_{max} values in the presence of sugars under the lowest ionic strength conditions, indicating that sugars improved the thermal stabilities of MAbs.

Electrostatic Potential Surfaces

The electrostatic potential surfaces of MAb-A and MAb-B were simulated as a function of ionic strength at pH 5 and pH 7, as shown in Fig. 5. The positive potential (+1 k_BT/e) and negative potential (-1 k_BT/e) isovalue surfaces are presented as blue and red areas, respectively. MAb-A at pH 5 and at an ionic strength of 40 mM had a positive potential surface over its structure except for the negative potential surface area around the CDR region (Fig. 5a). At pH 7 and an ionic strength of 40 mM, the negative potential surface increased slightly, whereas the positive potential surface decreased significantly and a negative potential surface appeared around the center of the molecule (Fig. 5c). In the case of MAb-B at pH 5 and an ionic strength of 10 mM, the large positive potential surface covered the entire structure and hardly any negative potential surface was observed (Fig. 5e). At pH 7, the positive potential surface decreased drastically, and small potential patches appeared around the center of the molecule (Fig. 5g). For all the MAbs, these distinct large potential surfaces observed at low ionic strength completely disappeared and many small potential surfaces appeared at an ionic strength of 310 mM (Fig. 5b, d, f, h).

Table II Effect of Sugars on Conformational Stability Assessed by Differential Scanning Calorimetry

pH	Formulation	T_{max} (°C)	
		MAb-A	MAb-B
5	Initial buffer	68.6	76.9
	+Sorbitol	69.7	77.7
	+Sucrose	70.1	78.0
	+Trehalose	70.6	77.9
7	Initial buffer	68.5	67.7
	+Sorbitol	69.2	74.4
	+Sucrose	69.6	74.8
	+Trehalose	69.6	74.8

The lowest ionic strength buffers (initial buffers) contained 30 mM NaCl for MAb-A and no NaCl for MAb-B

The standard deviation of T_{max} was approximately less than 0.1 °C

DISCUSSION

Relationship Between Colloidal Stability and Net Charge

Under accelerated storage conditions at 40°C, at which the MAbs maintained their folded state (Supplementary Material Figure S2), the aggregation propensities were in quantitatively good agreement with the colloidal stability assessed from the values of B_2 (Figs. 1 and 4). We first tried to interpret these observations according to DLVO theory, which accounts for the interaction between two identical molecules in solution. DLVO theory states that the dispersity of a molecule is determined by the sum of two major intermolecular forces, namely, charge–charge and van der Waals interactions. The van der Waals interactions are dispersive forces that are effective over shorter intermolecular distances than charge–charge interactions. The magnitude of intermolecular forces depends on the intermolecular distance between two molecules (42). For spherical colloidal particles, charge–charge and van der Waals interactions induce repulsive and attractive intermolecular interactions, respectively. Charge–charge interactions are long-range intermolecular interactions; they are inversely proportional to the intermolecular distance between two molecules and can be significant even at distances of 1.5–2.0 nm under conditions of low ionic strength (42). When the electrostatic repulsion is significantly greater than the van der Waals force, the molecules can stably disperse. Charge–charge interactions are directly related to the charge states on the surfaces of molecules and are affected by environmental conditions, such as the dielectric constants of the solvent

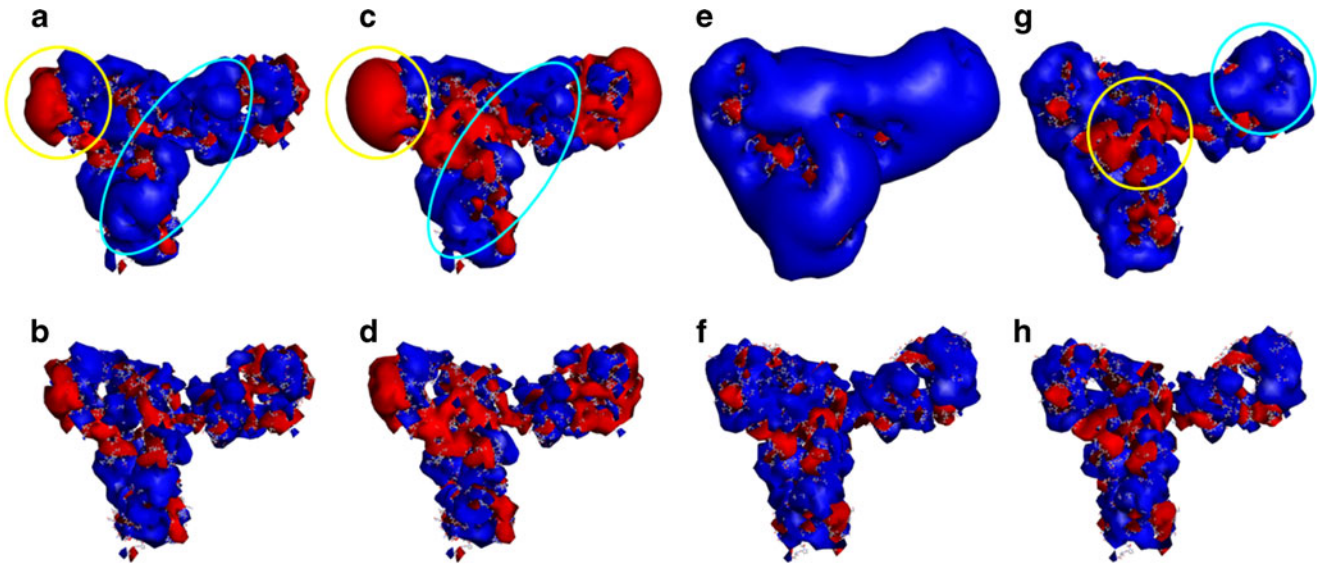

Fig. 5 Electrostatic potential surfaces of MAb-A and MAb-B at different ionic strengths and pHs (**a**, **b**) MAb-A at pH 5; (**c**, **d**) MAb-A at pH 7; (**e**, **f**) MAb-B at pH 5; (**g**, **h**) MAb-B at pH 7). (**a**, **c**, **e**, **g**) Electrostatic potential surface at the lowest ionic strength (40 mM ionic strength for MAb-A and 10 mM ionic strength for MAb-B); (**b**, **d**, **f**, **h**) those at an ionic strength of 310 mM. Isovalue surfaces are represented in blue and red as positive (+1 k_BT/e) and negative (-1 k_BT/e) charged surfaces, respectively.

and ionic solutes. We therefore determined the net charge to estimate the degree of electrostatic repulsion that enhances colloidal stability. In contrast to the recent report by Lehermayer *et al.* in which B_2 was shown to increase as the net charge increased, the correlation of net charge with B_2 holds in only a limited number of cases, and therefore, the aggregation propensity is not always predictable from the net charge (Figs. 3 and 4) (28). DLVO theory regards particles as spherical molecules with uniform charge distributions on their surfaces. In some cases, the localization of positive and negative charges are heterogeneous in proteins composed of multi-domains, such as MAbs. These uneven distributions of charge can induce attractive interactions even if the apparent net charge is positive. In MAb-A, the absolute values of the net charges were approximately +5 to +7 under low ionic strength at pH 5 and pH 7 (Fig. 3a). Increasing the NaCl concentration to 140 mM reduced the net charge to approximately +2 k_BT/e, that is one-third of that under low ionic strength. Contrary to the prediction based on the uniform charge distribution model, aggregation decreased as the NaCl concentration increased (Fig. 4a, b). These trends in aggregation propensities as a function of NaCl concentration were the inverse of the trends for the relationship to net charge. Thus, again, the net charge does not always reflect colloidal stability. Unexpectedly, the net charge was reduced by the addition of sugars. Cosolvents, including sugars, change the hydration state of proteins through a preferential hydration mechanism and/or preferential interaction between sugars and proteins (43–45), which might change the electrostatic state of MAbs.

Molecular Origins of Aggregation Propensities

In the present study, the MAbs showed distinct dependencies of B_2 on pH or ionic strength, as shown in Figs. 1 and 2, indicating that colloidal stability was sensitive to pH and ionic strength. The interaction between two protein molecules can be described by B_{22}:

$$B_{22} = -\frac{1}{2}\frac{N_A}{M_W^2}\int \left(e^{-W_{22}/k_BT} - 1\right)4\pi r^2 dr \tag{6}$$

where T is the temperature, r is the center-to-center separation of the two solute molecules, N_A is Avogadro's number, and W_{22} is described as follows:

$$W_{22}(r) = W_{hs}(r) + W_{charge}(r) + W_{disp}(r) + W_{osm}(r) + W_{dip}(r) + W_{ass}(r) \tag{7}$$

where W_{hs} represents the hard sphere potential, W_{charge} is the energetic potential comprising charge–charge interactions, W_{disp} is the dispersion (van der Waals) attractive potential, W_{osm} is the attractive potential resulting from the osmotic effect of high salt concentrations, W_{dip} represents the interactions arising from the permanent and induced dipole moments of the molecules, and W_{ass} is the square-well interaction, which accounts for protein self-association. The square-well potential results from strong short-range interactions, such as hydrophobic interactions, hydrogen bonds, and ionic bonds (46). This equation, Eq. 6, was originally proposed by McMillan and Mayer, and theoretical and experimental studies address the contribution of

each term to the overall potential (46–49). In Eq. 7 for W_{22}, W_{hs} and W_{charge} generate repulsive forces, while other potentials generate attractive forces. At concentrations of <10 mg/mL where B_2 was determined, the minimum average intermolecular distance between MAbs is 30 nm. At this concentration range, electrostatic repulsion (W_{charge}), which is a long-range interaction, is effective and the dominant contribution to W_{22} (42). The addition of salts suppresses electrostatic repulsion (W_{charge}), resulting in a reduction in colloidal stability. Aggregation and/or reductions in solubility are therefore promoted by increased salt concentrations. In our present study, MAb-B, MAb-C, and MAb-D demonstrated excellent colloidal stabilities at pH 5 with strong repulsive intermolecular interactions in the absence of NaCl as indicated by their high B_2 values [$B_2 > 40 \times 10^{-5}$ (mLmol)/g^2]. Significant suppression of repulsive forces was observed in the presence of 300 mM NaCl as apparent from the small B_2 values [$B_2 < 3 \times 10^{-5}$ (mLmol)/g^2]. Likewise, suppression of repulsive forces was observed in all MAbs at pH values resulting in positive B_2 values at low NaCl concentrations (Fig. 2). In these cases, W_{charge} contributes significantly to W_{22} as repulsive intermolecular interaction. The salt concentration in the formulation therefore requires minimization. Exceptionally, positive B_2 for MAb-D at pH 7, approximately 2×10^{-5} (mLmol)/g^2, was unchanged by the addition of NaCl (Fig. 2d). One possible explanation for the positive value of B_2 for MAb-D at pH 7, even under low ionic strength, is a contribution from the excluded volume instead of by electrostatic repulsion as discussed later.

W_{hs} might potentially contribute to the repulsive forces represented by W_{22}. The contribution of W_{hs} by each MAb to B_{22} was estimated using Eq. 8, describing the excluded volume (22):

$$B_{22} = \frac{16\pi N_A R_2^3}{3} + \frac{\mathcal{Z}_2^2(1 + 2\kappa R_2)}{4I(1 + \kappa R_2)^2} \quad (8)$$

where $\mathcal{Z}$ is the net charge, I is the ionic strength, and κ is the inverse screening length, calculated from the molar ionic strength as $3.27 \times 10^7\sqrt{\mathrm{I}}$ (cm^{-1}). The estimated values were approximately 4–5 $\times 10^{-5}$ (mLmol)/g^2, with the assumption that MAbs are spheres with a diameter of 9 nm. The contribution of excluded volume to B_2 are less than one-eighth of B_2 values [40×10^{-5} (mLmol)/g^2] of the MAbs with higher colloidal stability, such as in the cases of MAb-B, MAb-C, and MAb-D at pH 5. This indicates that the electrostatic repulsion (W_{charge}) is dominant in influencing colloidal stability at the lowest ionic strength. In contrast, at high ionic strength, W_{charge} contributes little to the repulsive forces, and W_{hs}, the excluded volume potential, becomes dominant for positive B_2 values. Notably, MAb-A at pH 5 and pH 6, and MAb-B, MAb-C, and MAb-D at all pH values had similar B_2 values, $0 < B_2 < 3 \times 10^{-5}$ (mLmol)/g^2, which were close to those estimated from the excluded volume, 4–5 $\times 10^{-5}$ (mLmol)/g^2, in the presence of 300 mM NaCl (Fig. 2). Exceptionally, in MAb-A at pH 7, the B_2 values [6×10^{-5} (mLmol)/g^2] were slightly higher than those calculated from the excluded volume. This phenomenon could be explained by findings that anion binding generates repulsive interactions among protein molecules (50–52). The marginally positive value of B_2 for MAb-A at pH 5 could also be attributed to binding of anions, which would mainly occur at positively charged patches on the MAb-A. Note the uneven charge distribution on the surface of MAb-A (Fig. 5a, c, also see discussion below). Considering the pI (6.7) of MAb-A, the total area of positively charged patches on MAb-A at pH 7 is smaller than that at pH 5 (Fig. 5a, c); therefore, anion binding is less effective at pH 5 than at pH 7.

When B_2 is negative at the lowest ionic strength like the cases of MAb-A at pH 5 and pH 7, and MAb-B at pH 7, according to Eq. 7, the possible contributions to attractive potentials are W_{disp}, W_{osm} W_{dip}, and W_{ass}. The osmotic attraction (W_{osm}) is not important at the low salt concentrations tested in the present study (46,53,54). Furthermore the dispersion force (W_{disp}) and the square-well interaction (W_{ass}) are short-range intermolecular interactions; therefore, they contribute little to attractive interactions at the concentrations used here. However, the dipole-related interaction (W_{dip}), which is effective over relatively long molecular distances, can play a dominant role in attractive interactions (47). Note that increases in NaCl concentration enhanced colloidal stability in some cases, such as that observed for MAb-A at all pH values, MAb-B and MAb-C at pH 7 and pH 8, and MAb-D at pH 8 (Fig. 2). Specifically, the stabilities of MAb solutions with negative B_2 values improved as the ionic strength increased. Such cases imply the presence of attractive dipolar electrostatic interactions that are progressively screened at higher salt concentrations. Salts, therefore, represent a two-edged sword, reducing or enhancing the colloidal stability depending on either repulsive or attractive intermolecular interaction.

Relationship Between Electrostatic Interactions and Electrostatic Potential Surfaces

The electrostatic potential surfaces simulated according to the Poisson–Boltzmann equation show uneven localizations of negative (-1 k_BT/e) and positive (+1 k_BT/e) potential surfaces, particularly for MAb-A at an ionic strength of 40 mM at pH 5. The positive potential surface covered most of the molecules, exception around the F_V region, where a negative potential surface was observed (Fig. 5a). This uneven localization of negative and positive potential surfaces is consistent with the large negative B_2 value [-8×10^{-5} (mLmol)/g^2] of MAb-A at

pH 5 under low salt conditions, suggesting the presence of dipolar attractive electrostatic interactions. Yadav *et al.* also suggested that uneven localizations of positive and negative potential surfaces were attributable to attractive interactions, resulting in viscosity enhancement (24,42). In contrast, MAb-B at pH 5 showed an evenly distributed electrostatic potential surface with the positive potential surface covering the entire structure, and hardly any negative potential surface was observed (Fig. 5e). The positive potential surface occupied a larger volume than the actual molecular size. This large positive potential surface is considered to contribute to strong repulsive intermolecular interactions. Indeed, the presence of strong repulsive interactions was indicated by the large positive B_2 values [$B_2 > 50 \times 10^{-5}$ (mLmol)/g^2], which require a large contribution from W_{charge}, as illustrated above, besides that from W_{hs} [5×10^{-5} (mLmol)/g^2] in Eq. 7.

The electrostatic potential surfaces at higher ionic strengths showed significant reductions in the large potential surfaces (Fig. 5b, d, f, h). The large potential surfaces disappeared and small potential surfaces were distributed sparsely over the molecule. The volume occupied by the potential surface became as small as the molecular size, in contrast to those at low ionic strengths. These potential surfaces contributed to the small repulsive intermolecular interactions, as indicated by B_2. These findings support the observation that the dispersity was enhanced by increasing the salt concentration for MAb-A at pH 5. Uneven localization of large negative and positive potential surfaces should therefore be eliminated to prevent attractive electrostatic interactions.

In the case of humanized IgG1, all MAbs have the same amino acid sequences and three-dimensional structures in a constant region; this provides a strong positive potential surface around pH 5–6, which is a condition frequently used for MAb formulations. Designing the amino acid sequence in the variable region avoids negative potentials and is therefore a promising approach of generating stable MAbs with low aggregation propensities. It should be noted that the positive potential surfaces that are dominant at pH 5 weaken at pH 7, and then negative potential surfaces appear in the constant region, resulting in uneven localization of the potential surfaces. Consistently, the presence of attractive interactions was indicated by B_2 for both MAb-A and MAb-B at pH 7. The simulation of the electrostatic potential surfaces should therefore be conducted with consideration of the pH and ionic strength.

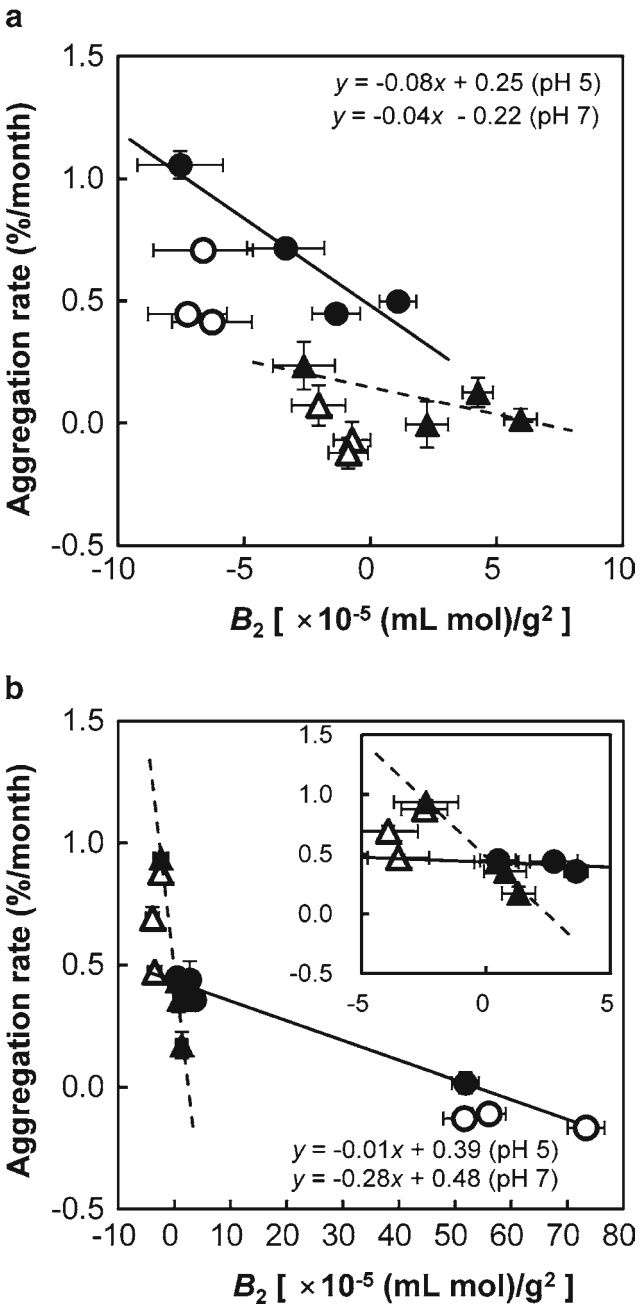

Fig. 6 Correlation of second virial coefficient B_2 with aggregation propensity for storage at 40°C of MAb-A (**a**) and MAb-B (**b**) at pH 5 (*circles*) and pH 7 (*triangles*); filled symbols represent formulations containing NaCl and open symbol represents formulations containing sugars. Linear regression was generated from formulations excluding those containing sugars. The correlation coefficients were R = -0.939 (MAb-A: pH 5), $R = -0.719$ (MAb-A: pH 7), $R = -0.986$ (MAb-B: pH 5), and $R = -0.992$ (MAb-B: pH 7). The error bar was estimated from three independent experiments performed under the same conditions.

Effects of Colloidal and Conformational Stabilities on Aggregation of MAbs Stored at 40°C

As shown in Fig. 6, linear correlations were observed between B_2 values and aggregation rates in the formulations containing different concentrations of NaCl, indicating that B_2 representing the colloidal stability well reflect the aggregation propensities for all the MAbs under accelerated storage condition at 40°C, which are normally used in stability tests. These results suggest that electrostatic interactions make major and quantitative contributions to the aggregation propensities

of these MAbs and can therefore be predicted from the experimental estimates of B_2. It is important to note that aggregation was suppressed almost completely when B_2 was sufficiently positive; empirically $B_2 > 40 \times 10^{-5}$ (mLmol)/g^2.

The B_2 values for the formulations containing sugars also corresponded well with the aggregation propensities. The aggregation rates were, however, slightly lower than the values predicted from B_2 for MAb-A (open symbols, Fig. 6). This stabilization effect by sugars is attributed to factors other than colloidal stability. The different aggregation pathways related to conformational stability should be considered, particularly heat-induced aggregation resulting from structural and chemical perturbations. The T_{max} values determined from the formulations containing sugars were higher than those in the initial buffer for all MAbs (Table II). These improvements in conformational stability contribute, in part, to the slight improvements in aggregation propensities in the presence of sugars for MAb-A at pH 5 and pH 7, and MAb-B at pH 7. To evaluate the relationship between the enhancement of T_{max} and the degree of increase in conformational stability, we calculated ΔG_{FU} at 40°C ($\Delta G_{FU,\ 313.15K}$) using ΔH, ΔC_P, and T_{max} obtained from DSC, assuming that the unfolding of MAbs occurs in a two-state manner. This calculation provides only a rough estimate, because MAbs unfold through multiple intermediates, which is different from the two-state unfolding of small proteins we studied previously (55). The 2 K difference in the T_{max} values of MAb-A in initial buffer (T_{max} = 68.8°C) and that in the buffer containing trehalose (T_{max} = 70.8°C) at pH 5 corresponds to a difference in $\Delta G_{FU,\ 313.15K}$ ($\Delta\Delta G_{FU,\ 313.15K}$) of 1.6 kcal/mol, implying that the population of unfolded molecules in the initial buffer is 10-times higher than that in the buffer containing 10% trehalose. This may contribute to the difference in the aggregation propensity after 4 weeks of storage at 40°C. Consistent with our estimate above, Kaushik and Bhat reported stabilization of lysozyme by 2.22 kcal/mol with 1 M (34%) trehalose (43). It should be noted that in the present study, the heat capacity change upon unfolding (Supplementary Material Figure S2), ΔC_P, was decreased by the addition of sugars. A decrease in ΔC_P generally results in a shallower dependence of ΔG_{FU} on temperature (43); therefore, the addition of sugars may stabilize MAbs over a broad range of temperature.

The T_{max} values for MAb-B at pH 5 were higher in the presence of sugars than those at the lowest ionic strength, whereas the stabilization effect was not observed in aggregation propensities. The T_{max} values MAb-B at pH 5 were higher than those determined under other conditions, indicating superior conformational stability even in the absence of sugars. This may explain why the contribution of conformational stability was not significant for MAb-B at pH 5.

In our previous and present studies, B_2 was measured at 20°C using AUC-SE (5). As already mentioned, the value of B_2 at 20°C correlated significantly with aggregation propensities at 40°C (Fig. 6). This result is consistent with findings that B_2 values at 20°C show a linear correlation with those determined for 40°C as shown in Fig. 7. The degree and type of intermolecular interactions are temperature-dependent, and the temperature dependencies of intermolecular interactions are influenced by the buffer components and proteins (56–58). However, in contrast to a study reporting a dramatic change in B_2 induced by a conformational change due to increasing temperature (59), the populations of MAbs in the unfolded state have similar B_2 values at 20°C and 40°C. Consequently, in the present study, the rank order and sign of B_2 values at two different temperatures are consistent with each other. Furthermore, aggregation rates at 40°C were in good agreement with those at 25°C (Supplementary Material Figure S3), confirming that determination of B_2 at 20°C accurately reflects the aggregation propensities at both temperatures.

Effects of Colloidal and Conformational Stability on Aggregation during Freeze–Thaw Cycles

Aggregation caused by freeze–thaw cycles is attributed to a combination of various stress factors such as cryo-concentration (60), cold denaturation (61), generation of an ice–solution interface (62), solute crystallization (63), and shifts in pH (64). Cryo-concentration and solute crystallization can potentially alter colloidal stability because of changes in the intermolecular distances between solutes and the ionic strength of the solution. In contrast, cold denaturation and adsorption to an ice–liquid interface alter the conformational stability by increasing the exposure of the hydrophobic residues buried in the proteins. Thus, aggregation under freeze–thaw stress needs to be assessed in terms of both conformational and colloidal stabilities.

The colloidal stability defined by B_2 failed to explain aggregation behaviors under freeze–thaw stress. This is evident for MAb-A at pH 5 and MAb-B at pH 7. Aggregation rates of MAb-A at pH 5 were effectively suppressed even in the presence of stronger attractive interactions (Figs. 4a and 8a). Similarly, significant suppression of aggregation was observed in the absence of NaCl in MAb-B at pH7, and B_2 was more attractive than those in the presence of NaCl (Figs. 4d and 8b). In contrast, the aggregation propensities of all MAbs were significantly improved by sugars, independent of B_2 values (open symbols, Fig. 8). Here, enhancements in T_{max} values were observed in the presence of sugars for MAb-A and MAb-B, which correlated qualitatively with aggregation propensities (Table II).

T_{max} reflects the conformational stability of the Fab domain of all MAbs (13,65). The reductions in aggregation propensities in the presence of sugars were therefore attributed to enhanced conformational stability of the Fab domain.

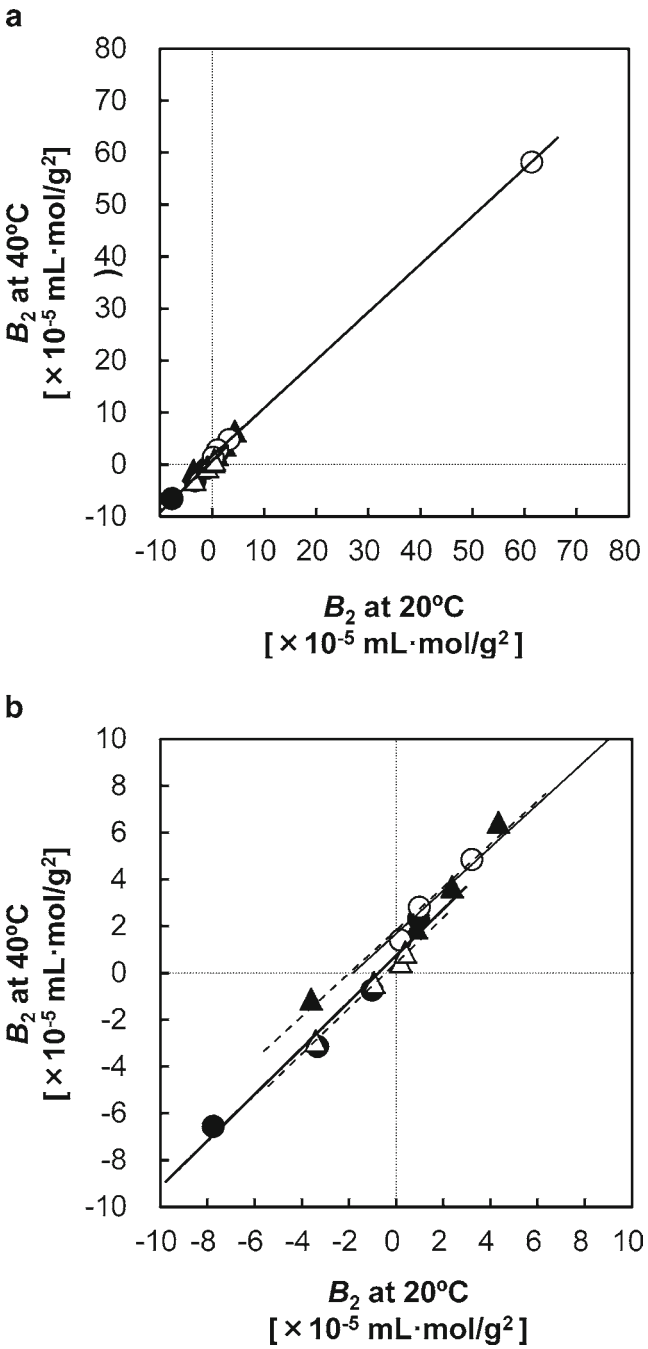

Fig. 7 Correlation of second virial coefficient, B_2, at 20°C and 40°C for MAb-A at pH 5 (*closed circle, solid line*), MAb-A at pH 7 (*closed triangle, dotted line*), MAb-B at pH 5 (*open circle, solid line*), and MAb-B at pH 7 (*open triangle, dotted line*). The correlation coefficients are $R = 0.987$ (MAb-A: pH 5), $R = 0.982$ (MAb-A: pH 7), $R = 1.000$ (MAb-B: pH 5), and $R = 0.998$ (MAb-B: pH 7).

Preferentially excluded sugars stabilize protein conformations by localizing water molecules around the protein (38), resulting in a lower aggregation propensity. This stabilizing effect might play a major role on suppressing the unfolding at the liquid-ice interface boundary under freeze–thaw stress. Although the relationship between unfolding induced by an increase in temperature and those caused by contact with a hydrophobic interface was not fully elucidated here, our results suggest that conformational stability correlates with aggregation under freeze–thaw stress. Unlike sugars, T_{max}

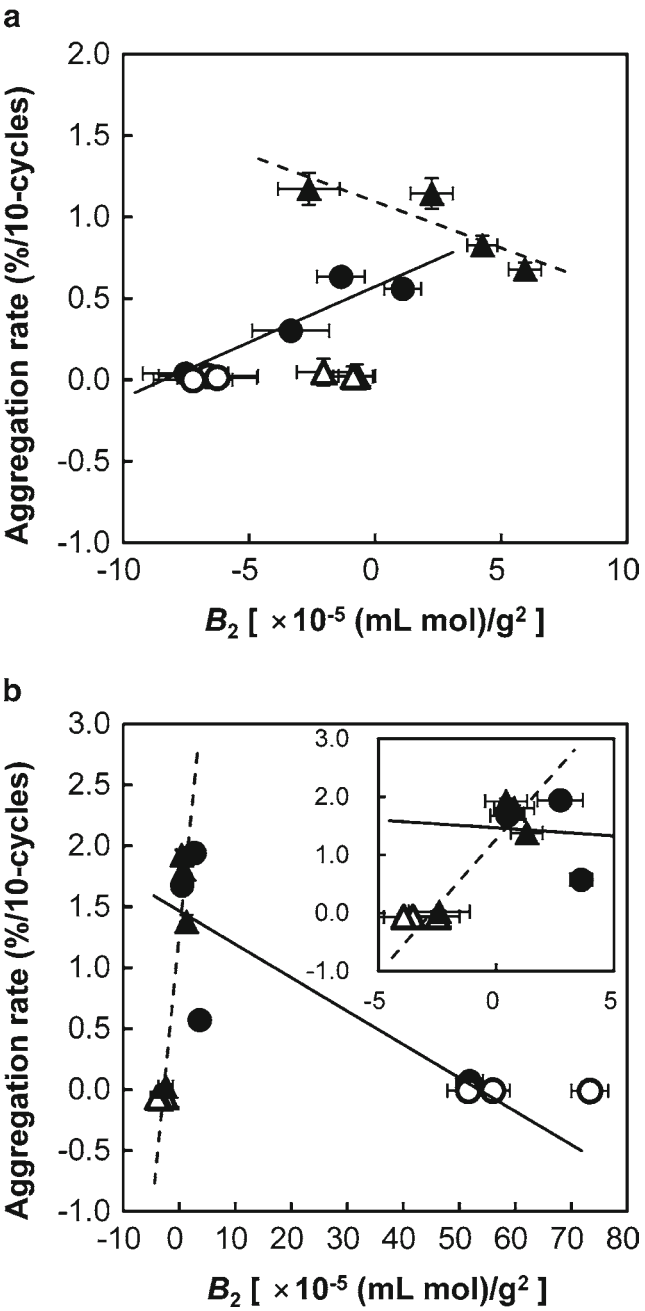

Fig. 8 Correlation of second virial coefficient B_2 with aggregation propensity under freeze–thaw cycles of MAb-A (**a**) and MAb-B (**b**) at pH 5 (*circles*) and pH 7 (*triangles*); *filled symbols* represent formulations containing NaCl and open symbols represent formulations containing sugars. The correlation coefficients from all formulations, excluding those containing sugars, were $R = 0.921$ (MAb-A: pH 5), $R = -0.869$ (MAb-A: pH 7), $R = -0.765$ (MAb-B: pH 5), and $R = 0.882$ (MAb-B: pH 7). The error bar was estimated from three independent experiments performed under the same conditions.

values obtained from buffers containing different concentrations of NaCl did not show clear correlations with aggregation propensities (data not shown). Thus, the relationships of colloidal and conformational stabilities with aggregation under freeze–thaw stress in the presence of salts has not been clarified and requires further investigation.

General Strategy for Formulation Optimization of MAbs

We suggest an effective strategy for the selection of optimum MAb formulations according to our current study together with previous studies. Colloidal stability correlates significantly with aggregation propensity under storage at 40°C and is strongly influenced by changes in salt concentration, because electrostatic interactions have a large effect on colloidal stability. The optimization of electrostatic interactions is therefore performed as a first step in the selection of the optimum formulation. Here, the formulation is selected to suppress electrostatic attraction and to enhance electrostatic repulsion.

In a practical experiment, B_2 is first measured at low ionic strength at acidic and neutral pHs. The solution with the pH providing the largest B_2 is selected. If B_2 is positive at the desired pH, salts should not be added, because their addition would lead to a reduction in colloidal stability by cancelling favorable electrostatic repulsions. If B_2 is negative at the desired pH, salts can be added to improve the colloidal stability by cancelling the electrostatic attractions. In the present study, MAb-B, MAb-C, and MAb-D at pH 5 are the preferred formulations and are characterized by very large B_2 values.

The second step is the selection of sugars to improve the conformational stability. Basically, sugars are added to improve the freeze–thaw stability. In the experiment, T_{max} (T_m of the Fab fragment) measurements using DSC are performed in selected formulations containing various sugars. The sugars providing the highest T_{max} would be the first choice, although all sugars that we tested differed only slightly in their ability to improve stability.

As a final step, assessment of stability is performed to directly measure the aggregation propensity. In formulation development, restrictions in osmolality are often required, depending on the dosage form. Therefore, if necessary, screening for different combinations of various concentrations of salts and sugars is effective. In summary, the optimum formulation is selected according to the following steps: [1] optimization of pH and salts on the basis of colloidal stability, [2] selection of sugar on the basis of conformational stability, and [3] direct stability assessment of the selected formulation. This proposed approach reduces the burden of direct stability assessment, which is time consuming and requires a large amount of sample. In practice, an optimum formulation for MAb-A can be predicted according to this strategy. The B_2 value for MAb-A was larger at pH 7 than at pH 5 in the presence of low concentrations of NaCl. The B_2 value was negative even at pH 7, indicating the presence of attractive intermolecular interactions. A formulation containing salts is therefore selected. Moreover, sugars are added to improve the freeze–thaw stability and to enhance conformational stability (Supplementary Material Figure S4), providing a higher T_{max}. The selected formulation is at pH 7 and contains salts and sugars. The concentrations and types of salts and sugars are optimized in the final step. The tentative formulation is the same as the formulation providing the lowest aggregation propensities for storage at 40°C and under freeze–thaw stress. For MAb-B, a larger B_2 is obtained at pH 5. The B_2 value is positive at pH 5; therefore, only sugars are added. The selected formulation is at pH 5, containing sugars but not salts. This formulation is also the same as that providing the lowest aggregation propensities for storage at 40°C and under freeze–thaw stress.

MAb-A and MAb-B represent typical types of MAbs, and specifically, MAb-A and MAb-B have unevenly and evenly distributed electrostatic potential surfaces, respectively. MAb-A showed higher colloidal stability in the presence of salts, whereas the trend for MAb-B was the opposite. Our strategy for optimization is applicable for both types of MAbs and can be generalized.

CONCLUSION

Elucidation of the aggregation mechanism and prediction of aggregation propensity are considerable challenges because multiple pathways, which are influenced by various stress factors, contribute in different degree to aggregation. In the present study, in order to develop optimization strategy for MAb formulation we evaluated colloidal and conformational stabilities of MAbs and then confirmed their relations to the aggregation behaviors. The colloidal stabilities were accurately assessed according to B_2 values obtained from AUC-SE. The net charge reflected the magnitude of the electrostatic interactions, but only partly correlate with the colloidal stability; as observed in the present study, the electrostatic attraction and repulsion contributed oppositely to colloidal stability. Salts both stabilize and destabilize the MAbs, depending on the type of electrostatic interaction, *i.e.*, repulsion or attraction. Proper determination of the intermolecular interactions is therefore of great importance for optimizing salts in formulations. The electrostatic potential surfaces showed that an uneven localization of potential surfaces contributed to attractive interactions, resulting in higher aggregation propensities. In contrast, evenly distributed potential surface induced strong repulsive intermolecular

interactions. Sugars did not have a significant influence on the colloidal stabilities but improved aggregation propensities at 40°C and under freeze–thaw stress mainly by improving the conformational stability of the Fab fragment. The colloidal and conformational stabilities therefore both contributed to aggregation to different degrees, depending on the stress factors.

In summary, assessment of colloidal stability at the lowest ionic strength is particularly effective for the formulation development. If necessary, salts are added to enhance the colloidal stability. Sugars further improve the aggregation propensities, in particular under the freeze–thaw stress, by enhancing conformational stability. These behaviors are rationally predictable according to the potential surfaces of MAbs.

ACKNOWLEDGMENTS AND DISCLOSURES

The authors would like to thank Tetsuya Shiozaki, Daisuke Ama, Kei Kubota, Yuki Araki, Yuki Shioiri and Mikiya Yamanaka (Daiichi Sankyo Co., Ltd., Tokyo, Japan) for their skillful technical support.

REFERENCES

1. Rosenberg AS. Effects of protein aggregates: an immunologic perspective. AAPS J. 2006;8(3):E501–7.
2. Mahler HC, Friess W, Grauschopf U, Kiese S. Protein aggregation: pathways, induction factors and analysis. J Pharm Sci. 2009;98(9):2909–34.
3. Chi EY, Krishnan S, Randolph TW, Carpenter JF. Physical stability of proteins in aqueous solution: mechanism and driving forces in nonnative protein aggregation. Pharm Res. 2003;20(9):1325–36.
4. Hawe A, Kasper JC, Friess W, Jiskoot W. Structural properties of monoclonal antibody aggregates induced by freeze–thawing and thermal stress. Eur J Pharm Sci. 2009;38:79–87.
5. Saito S, Hasegawa J, Kobayashi N, Kishi N, Uchiyama S, Fukui K. Behavior of Monoclonal Antibodies: Relation Between the Second Virial Coefficient (B_2) at Low Concentrations and Aggregation Propensity and Viscosity at High Concentrations. Pharm Res. 2012;29(2):397–410.
6. Chi EY, Krishnan S, Kendrick BS, Chang BS, Carpenter JF, Randolph TW. Roles of conformational stability and colloidal stability in the aggregation of recombinant human granulocyte colony-stimulating factor. Protein Sci. 2003;12:903–13.
7. Goldberg DS, Bishop SM, Shah AU, Sathish HA. Formulation development of therapeutic monoclonal antibodies using high-throughput fluorescence and static light scattering techniques: role of conformational stability and colloidal stability. J Pharm Sci. 2011;100(4):1306–15.
8. Chou DK, Krishnamurthy R, Manning MC, Randolph TW, Carpenter JF. Physical stability of albinterferon-α_{2b} in aqueous solution: effects of conformational stability and colloidal stability on aggregation. J Pharm Sci. 2012;101(8):2702–19.
9. Zhang J, Liu XY. Effect of protein-protein interactions on protein aggregation kinetics. J Chem Phys. 2003;119(20):10972–6.
10. Saluja A, Kalonia DS. Nature and consequences of protein-protein interactions in high protein concentration solutions. Int J Pharm. 2008;358:1–15.
11. Verwey EJW, Overbeck JTK. Theory of stability of lyophobic colloids. Amsterdam: Elsevier; 1948.
12. Zhang A, Singh SK, Shirts MR, Kumar S, Fernandez EJ. Distinct aggregation mechanisms of monoclonal antibody under thermal and freeze–thaw stresses revealed by hydrogen exchange. Pharm Res. 2012;29:236–50.
13. Garber E, Demarest SJ. A broad range of Fab stabilities within a host of therapeutic IgGs. Biochem Biophys Res Commun. 2007;355:751–7.
14. Neal BL, Asthagiri D, Lenhoff AM. Molecular origins of osmotic second virial coefficients of proteins. Biophys J. 1998;75:2469–77.
15. Liu J, Nguyen MDH, Andya JD, Shire SJ. Reversible self-association increases the viscosity of a concentrated monoclonal antibody in aqueous solution. J Pharm Sci. 2005;94(9):1928–40.
16. Attri AK, Minton AP. New methods for measuring macromolecular interactions in solution *via* static light scattering: basic methodology and application to nonassociating and self-associating proteins. Anal Biochem. 2005;337:103–10.
17. Alford JR, Kendrick BS, Carpenter JF, Randolph TW. Measurement of the second osmotic virial coefficient for protein solutions exhibiting monomer-dimer equilibrium. Anal Biochem. 2008;377:128–33.
18. Tessier PM, Lenhoff AM, Sandler SI. Rapid measurement of protein osmotic second virial coefficients by self-interaction chromatography. Biophys J. 2002;82:1620–31.
19. Brun VL, Friess W, Bassarab S, Mühlau S, Garidel P. A critical evaluation of self-interaction chromatography as a predictive tool for the assessment of protein-protein interactions in protein formulation development: a case study of a therapeutic monoclonal antibody. Eur J Pharm Biopharm. 2010;75(1):16–25.
20. Sule SV, Cheung JK, Antochshuk V, Bhalla AS, Narasimhan C, Blaisdell S. Solution pH that minimizes self-association of three monoclonal antibodies is strongly dependent on ionic strength. Mol Pharm. 2012;9:744–51.
21. Jiménez M, Rivas G, Minton AP. Quantitative characterization of weak self-association in concentrated solutions of immunoglobulin G *via* the measurement of sedimentation equilibrium and osmotic pressure. Biochemistry. 2007;46:8373–8.
22. Winzor DJ, Deszczynski M, Harding SE, Wills PR. Nonequivalence of second virial coefficients from sedimentation equilibrium and static light scattering studies of protein solutions. Biophys Chem. 2007;128:46–55.
23. Holde KE, Johnson C, Ho PS. Principles of physical biochemistry. Upper Saddle River: Pearson Education; 2006.
24. Yadav S, Laue TM, Kalonia DS, Singh SN, Shire SJ. The influence of charge distribution on self-association and viscosity behavior of monoclonal antibody solutions. Mol Pharm. 2012;9:791–802.
25. Yadav S, Shire SJ, Kalonia DS. Factors affecting the viscosity in high concentration solutions of different monoclonal antibodies. J Pharm Sci. 2010;99(12):4812–29.
26. Nishi H, Miyajima M, Nakagami H, Noda M, Uchiyama S, Fukui K. Phase separation of an IgG1 antibody solution under a low ionic strength condition. Pharm Res. 2010;27(7):1348–60.
27. Saluja A, Fesinmeyer M, Hogan S, Brems DN, Gokarn YR. Diffusion and sedimentation interaction parameters for measuring the second virial coefficient and their utility as predictors of protein aggregation. Biophys J. 2010;99:2657–65.
28. Lehermayr C, Mahler HC, Mäder K, Fischer S. Assessment of net charge and protein-protein interactions of different monoclonal antibodies. J Pharm Sci. 2011;100(7):2551–62.
29. Jachimska B, Wasilewska M, Adamczyk Z. Characterization of globular protein solutions by dynamic light scattering, electrophoretic

mobility, and viscosity measurements. Langmuir. 2008;24(13): 6866–72.
30. Nishi H, Miyajima M, Wakiyama N, Kubota K, Hasegawa J, Uchiyama S, *et al.* Fc domain mediated self-association of an IgG1 monoclonal antibody under a low ionic strength condition. J Biosci Bioeng. 2011;112(4):326–32.
31. Salinas BA, Sathish HA, Bishop SM, Harn N, Carpenter JF, Randolph TW. Understanding and modulating opalescence and viscosity in a monoclonal antibody formulation. J Pharm Sci. 2010;99(1):82–93.
32. Moody TP, Kingsbury JS, Durant JA, Wilson TJ, Chase SF, Laue TM. Valence and anion binding of bovine ribonuclease A between pH 6 and 8. Anal Biochem. 2005;336:243–52.
33. Durant JA, Chen C, Laue TM, Moody TP, Allison SA. Use of T4 lysozyme charge mutants to examine electrophoretic models. Biophys Chem. 2002;101–102:593–609.
34. Chase SF, Laue TM. The determination of protein valence by capillary electrophoresis. P/ACE Setter. 2008;12(1):1–5.
35. Harn N, Allan C, Oliver C, Middaugh CR. Highly concentrated monoclonal antibody solutions: direct analysis of physical structure and thermal stability. J Pharm Sci. 2007;96(3):532–46.
36. Vermeer AWP, Norde W. The thermal stability of immunoglobulin: unfolding and aggregation of a multi-domain protein. Biophys J. 2000;78(1):394–404.
37. Thakkar SV, Joshi SB, Jones ME, Sathish HA, Bishop SM, Volkin DB, *et al.* Excipients differently influence the conformational stability and pretransition dynamics of two IgG1 monoclonal antibodies. J Pharm Sci. 2012;101(9):3062–77.
38. Timasheff SN. Protein hydration, thermodynamic binding, and preferential hydration. Biochemistry. 2002;41(46):13473–82.
39. Laue TM, Shah BD, Ridgeway TM, Pelletier SL. Analytical ultracentrifugation in biochemistry and polymer science. London: Royal Society of Chemistry; 1992. p. 90–125.
40. Yadav S, Sreedhara A, Kanai S, Liu J, Lien S, Lowman H, *et al.* Establishing a link between amino acid scequence and self-associating and viscoelastic behavior of two closely related monoclonal antibodies. Pharm Res. 2011;28:1750–64.
41. Engelsman J, Garidel P, Smulders R, Koll H, Smith B, Bassarab S, *et al.* Strategies for the assessment of protein aggregates in pharmaceutical biotech product development. Pharm Res. 2011;28 (4):920–33.
42. Chari R, Jerath K, Badkar AV, Kalonia DS. Long- and short-range electrostatic interactions affect the rheology of highly concentrated antibody solutions. Pharm Res. 2009;26(12):2607–18.
43. Kaushik JK, Bhat R. Why is trehalose an exceptional protien stabilizer? J Biol Chem. 2003;278(29):26458–65.
44. Timasheff SN. Control of protein stability and reactions by weakly interacting cosolvents: the simplicity of the complicated. Adv Protein Chem. 1998;51:355–432.
45. Liu Y, Bolen DW. The peptide backbone plays a dominant role in protein stabilization by naturally occurring osmolytes. Biochemistry. 1995;34:12884–91.
46. Curtis RA, Prausnitz JM, Blanch HW. Protein-protein and protein-salt interactions in aqueous protein solutions containing concentrated electrolytes. Biotech Bioeng. 1998;57(1):11–21.
47. Elcock AH, McCammon JA. Calculation of weak protein-protein interactions: the pH dependence of the second virial coefficient. Biophys J. 2001;80(2):613–25.
48. McMillan Jr WG, Mayer JE. The statistical thermodynamics of multicomponent systems. J Chem Phys. 1945;13:276–305.
49. Kumar V, Dixit N, Zhou L, Fraunhofer W. Impact of short range hydrophobic interactions and long range electrostatic forces on the aggregation kinetics of a monoclonal antibody and a dual-variable domain immunoglobulin at low and high concentrations. Int J Pharm. 2011;421:82–93.
50. Fesinmeyer RM, Hogan S, Saluja A, Brych SR, Kras E, Narhi LO, *et al.* Effect of ions on agitation- and temperature-induced aggregation reactions of antibodies. Pharm Res. 2009;26(4):903–13.
51. Collins KD. Charge density-dependent strength of hydration and biological structure. Biphys J. 1997;72:65–76.
52. Collins KD. Ions from the Hofmeister series and osmolytes: effects on proteins in solution and in the crystallization process. Methods. 2004;34:300–11.
53. Asakura S, Oosawa F. On interaction between two bodies immersed in a solution of macromolecules. J Chem Phys. 1954;22:1255–6.
54. Asakura S, Oosawa F. Interaction between particles suspended in solutions of macromolecules. J Polym Sci. 1958;33:183–92.
55. Uchiyama S, Hasegawa J, Tanimoto Y, Moriguchi H, Mizutani M, Igarashi Y, *et al.* Thermodynamic characterization of variants of mesophilic cytochrome c and its thermophilic counterpart. Protein Eng Des Sel. 2002;15(6):455–61.
56. Burn VL, Friess W, Schultz-Fademrecht T, Muehlau S, Garidel P. Lysozyme-lysozyme self-interactions as assessed by the osmotic second virial coefficient: Impact for physical protein stabilization. Biotechnol J. 2009;4:1305–19.
57. Valente JJ, Payne RW, Manning MC, Wilson WW, Henry CS. Colloidal behavior of proteins: effects of the second virial coefficient on solubility, crystallization and aggregation of proteins in aqueous solution. Curr Pharm Biotechnol. 2005;6(6):427–36.
58. Antipova AS, Semenova MG, Belyakova LE. Effect of sucrose on the thermodynamic properties of ovalbumin and sodium caseinate in bulk solution and at air–water interface. Colloids Surf B Biointerface. 1999;12:261–70.
59. Burn VL, Friess W, Bassarab S, Garidel P. Correlation of protein-protein interactions as assessed by affinity chromatography with colloidal protein stability: a case study with lysozyme. Pharm Dev Technol. 2010;15(4):421–30.
60. Kueltzo LA, Wang W, Randolph TW, Carpenter JF. Effects of solution conditions, processing parameters, and container materials on aggregation of a monoclonal antibody during freeze–thawing. J Pharm Sci. 2008;97(5):1801–12.
61. Griko YV, Privalov PL, Sturtevant JM, Venyaminov SY. Cold denaturation of staphylococcal nuclease. Proc Natl Acad Sci USA. 1988;85:3343–7.
62. Chang BS, Kendrick BS, Carpenter JF. Surface-induced denaturation of proteins during freezing and its inhibition by surfactants. J Pharm Sci. 1996;85(12):1325–30.
63. Izutsu K, Yoshioka S, Terao T. Effect of mannitol crystallinity on the stabilization of enzymes during freeze-drying. Chem Pharm Bull. 1994;42(1):5–8.
64. Murase N, Franks F. Salt precipitation during the freeze-concentration of phosphate buffer solutions. Biophys Chem. 1989;34(3):293–300.
65. Welfle K, Misselwitz R, Hausdorf G, Höhne W, Welfle H. Conformation, pH-induced conformational changes, and thermal unfolding of anti-p24 (HIV-1) monoclonal antibody CB4-1 and its Fab and Fc fragments. Biochim Biophys Acta. 1999;1431(1):120–31.